

Selected Paper

Shape Selective Oxidative Etching and Growth of Single-Twin Plate-Like and Multiple-Twin Decahedral and Icosahedral Gold Nanocrystals in the Presence of Au Seeds under Microwave Heating

Masaharu Tsuji,*[1,2] Nobuhiro Miyamae,[2] Michiko Nishio,[2] Sachie Hikino,[1] and Naoki Ishigami[2]

[1]Institute for Materials Chemistry and Engineering, Kyushu University, Kasuga 816-8580

[2]Department of Applied Sciences for Electronics and Materials, Graduate School of Engineering Sciences, Kyushu University, Kasuga 816-8580

Received February 27, 2007; E-mail: tsuji@cm.kyushu-u.ac.jp

Shape- and size-controlled synthesis of gold nanocrystals was studied by using a microwave–polyol method in the presence of Au seeds and poly(vinylpyrrolidone) (PVP) as a polymer surfactant. Mixtures of spherical, triangular, hexagonal, octahedral, and decahedaral particles were prepared as Au seeds by reducing Au^{3+} in $AuCl_4^-$ in ethylene glycol (EG). When Au nanoparticles were prepared from $AuCl_4^-/Cl^-$/PVP/EG solutions by using these Au seeds, significant changes in shapes and sizes of the Au seeds occurred. Such changes depended strongly on the concentrations of $AuCl_4^-$ and Cl^-. Large single-twin plate-like particles and multiple-twin decahedral particles were the major products at high concentrations of $AuCl_4^-$, whereas icosahedral particles were preferentially produced at high Cl^- concentrations. It should be noted that the octahedral and spherical particles involved in the Au seeds were completely dissolved at high $AuCl_4^-$ and Cl^- concentrations. The significant changes in shapes and sizes of Au nanoparticles could be explained by the oxidative etching of the Au seeds by $AuCl_4^- + Cl^-$ anions in the range of 60–160 °C and crystal growth of specific shapes of Au nanocrystals in the range of 160–198 °C on the basis of changes in color and UV–vis–NIR spectra of solutions and TEM images of products during etching.

In recent years, a variety of metallic nanostructures, including spherical particles, sheets, plates, rods, wires, tubes, and dendrites, have generated significant scientific and technological interest, because of their unique optical properties as well as novel chemical and catalytic properties. Here, we define nanosheets as thin nanoplates with a thickness less than about 10 nm, and nanorods and nanowires as materials with aspect ratios of 2–20 and >20, respectively. The polyol method is a typical technique to prepare metallic nanoparticles in solutions by reducing their ionic salts. In general, a mixture of reagent and polymer surfactant in ethylene glycol (EG) is heated in an oil bath for several hours and spherical nanoparticles form.[1–3] Recently, microwave (MW) heating has been coupled with the polyol method as a new rapid preparation method for metallic nanoparticles. This method, named MW–polyol method, has been applied to the synthesis of various kinds of monometallic and bimetallic nanoparticles, as shown in our recent review.[4]

Among many metallic nanoparticles, gold nanoparticles have attracted intensive attention, not only because of their unique physical and chemical properties but also because of their important applications in catalysis, photoelectronic devices, and biomedicine.[5–9] It is well known that some chemical and physical properties and application of materials are dependent, to a large extent, on their shapes and sizes. Thus, many efforts have been made to find effective synthetic methods to prepare Au nanoparticles with different shapes and sizes.

We have recently applied the MW–polyol method to the rapid synthesis of Au nanostructures.[4,10–12] When Au^{3+} in $AuCl_4^-$ ions is reduced in EG in the presence of a polymer surfactant poly(vinylpyrrolidone) (PVP) under MW heating for 2–3 min, mixtures of triangular, square, rhombic, and hexagonal nanoparticles are produced preferentially. In addition, small numbers of one-dimensional (1-D) nanorods and nanowires are produced. For comparison, Au nanostructures have also been prepared under the conventional oil-bath heating,[4,10] and larger spherical nanoparticles are dominantly produced, indicating that the MW–polyol method gives higher crystalline Au nanoparticles than the oil-bath heating. The rapid preparation of higher crystalline Au nanoparticles under MW heating probably arises from the local heating of PVP covered on the Au particles, heating of polar reagent $AuCl_4^-$ anions, and/or the heating of free electrons in Au metallic nanoparticles (conduction loss).[13] To determine optimum experimental conditions for the synthesis of specific nanostructures, dependences of the shapes and the sizes on such experimental parameters as concentrations of $HAuCl_4 \cdot 4H_2O$ and PVP, molecular weights of PVP (10, 40, and 360 k), and solvents (EG and H_2O) have been examined.[4] We have found that the shapes and the sizes of the Au nanostructures depended strongly on these experimental parameters. However, further experimental techniques are required for the shape- and size-controlled synthesis of various Au nanocrystals.

We have recently extended our studies of MW–polyol synthesis of metallic nanostructures to Au@Ag core–shell nanocrystals.[14,15] For the preparation of Au@Ag nanocrystals, Au core crystals are synthesized by reduction of $HAuCl_4 \cdot 4H_2O$

Published on the web October 12, 2007; doi:10.1246/bcsj.80.2024

in the presence of PVP in the first step, and then $AgNO_3$ is reduced for the overgrowth of Ag shells in the second step. The crystal structures of Au cores and Au@Ag core–shell particles have been analyzed by observing the transmittance electron microscope (TEM) images from different view angles, selected area electron diffraction (SAED) patterns, and energy dispersive X-ray spectroscopy (EDS). Detailed data on crystal structures of Au cores show that Au particles, observed as polygonal plates, rods, and wires in our previous studies,[4,10] are mixtures of single-twin triangular plate, octahedral, and multiple-twin decahedral particles, surrounded by only {111} facets. We have discovered that triangular bipyramid, cubic, and rod/wire Ag shells, having {100} facets, are selectively grown over the above Au core crystals. It has been concluded that the morphology changes between Au core and Ag shell in Au@Ag particles arise from changes in the adsorption selectivity of PVPs from {111} facets of Au to {100} facets of Ag.

In the present study, Au particles were prepared by using the MW–polyol method in the presence of Au seeds under various experimental procedures to find the optimum experimental procedure and conditions for controlling the shape and the size of the Au nanocrystals. Among various experimental parameters, we focused here upon concentrations of $AuCl_4^-$ from $HAuCl_4 \cdot 4H_2O$ and Cl^- from $HAuCl_4$ and NaCl. It was found that these parameters played a significant role in the crystal growth of specific Au nanostructures. We found that favorable crystal structures of Au prepared using Au seeds were different from those of Au@Ag core–shell nanocrystals, even though Au and Ag have the same FCC structure and similar lattice constants.

It is well known that oxidative etching by halogen anion (e.g. Cl^-) in the presence of O_2 (dissolved in solvent) and Fe_3^+ play a significant role in controlling the shape and the size of Ag nanocrystals.[16] It has been thought that Au is more resistant to oxidative etching than Ag is, and it is, therefore, insoluble in most acids except for complete dissolution in an aqua regia. However, it has recently been reported that oxidative etching of gold nanoparticle occurs in such systems as Au^{III}–cetyltrimethylammonium bromide (CTAB) and Au^{III}–cyanide.[17,18] By spatially directed or undirected etching, spherical, rods, and multipods types of Au nanoparticles, having unique optical properties, have been synthesized.

We observed here that shape selective etching of Au seeds by $AuCl_4^- + Cl^-$ anions occurred in the $AuCl_4^-/Cl^-$/PVP/EG system. As a result, single-twin triangular plate-like particles and multiple-twin decahedral and icosahedral particles preferentially formed at high $AuCl_4^- + Cl^-$ concentrations. The etching and growth mechanisms of each Au seed are discussed based on TEM images and ultraviolet, visible, and near-infrared (UV–vis–NIR) absorption spectral data and color changes between reagent and product solutions at various temperatures. In order to clarify oxidative etching mechanism of Au seeds by $AuCl_4^- + Cl^-$ anions and effects of MW irradiation, Au nanoparticles were also prepared by using conventional oil-bath heating. We found for the first time that the etching rate of Au seeds under MW heating was faster than that in the oil-bath heating. The effects of MW irradiation for the etching of Au seeds are discussed.

Seeded growth of anisotropic Au nanoparticles from $HAuCl_4$ has been studied at room temperature using $NaBH_4$ as a reducing agent and CTAB as a capping agent.[6–8] In general, Au atoms are overgrown on small Au seeds, and the shapes and the sizes of Au seeds do not change during the preparation of anisotropic Au nanoparticles. In the present study, seeded growth of Au nanoparticles was studied by using a MW–polyol method. The present seeded growth system was significantly different from the above process, because the shapes and the sizes of Au seeds changed significantly due to shape selective etching before crystal growth at higher temperatures under MW heating.

Experimental

The MW–polyol method used in this study was similar to that reported previously.[4,10] We used $HAuCl_4 \cdot 4H_2O$ as sources of Au nanoparticles and Cl^- anons, PVP (molecular weight of 40000 in terms of monomeric units) as a protecting agent, NaCl as a source of Cl^- ions, and EG as both solvent and reductant. Mixtures of $HAuCl_4 \cdot 4H_2O$ (2.4 mM)/PVP (1 M) were resolved in 20 mL of EG solution. They were heated by MW irradiation in a continuous wave mode (Shikoku Keisoku: 400 W).[4,10] In this condition, the solution was rapidly heated from a room temperature to the boiling point of EG (198 °C) after about 1 min and held in this temperature for 2 min, when the temperature was monitored by using an optical fiber thermometer. The total heating time was generally 3 min. The product solution was used as an Au seed solution. In the Au seed solution, besides PVP (1 M), Cl^- anions, produced through the decomposition of $HAuCl_4$, may be involved. The concentration of Cl^- was determined to be 3.3 mM by using a titration apparatus (Kyoto Electronic AT610) with a standard $AgNO_3$ solution serving as the titration reagent. The lack of residual $AuCl_4^-$ anions after MW heating was confirmed by the disappearance of absorption band of $AuCl_4^-$ anion complex at ≈322 nm. Thus, the Au seed solution could be described as Au(seeds)/Cl^- (3.3 mM)/PVP (1 M)/EG system. If 2.4 mM of $AuCl_4^-$ anions is completely decomposed via process (1), the Cl^- concentration is expected to be 2.4 mM:

$$AuCl_4^- \rightarrow Au^0 + Cl_2 + Cl + Cl^-. \quad (1)$$

Thus, 38% of Cl in process (1) was converted to Cl^- via a subsequent $Cl + e^-$ reduction process (2) in solution:

$$Cl + e^- \rightarrow Cl^-. \quad (2)$$

In order to remove the small amount of residual Cl^- anions, the Au seed solution was centrifuged at 13000 rpm for 60 min, and the surfactant Cl^- anions and PVP in EG were removed. Then, a mixture of Au seeds and PVP (1 M) in fresh EG solution, denoted as Au(seeds)/PVP (1 M)/EG, was prepared by the addition of 20 mM of EG containing 1 M of PVP to Au seeds. The following four experiments were carried out to examine etching and growth mechanisms of Au nanocrystal seeds.

Procedure (1). This procedure was used for the study of effects of $AuCl_4^-$ anions by the addition of $HAuCl_4 \cdot 4H_2O$. Au(seeds)/$AuCl_4^-$ (2.4–21.6 mM)/Cl^- (3.3 mM)/PVP/EG solutions were prepared by the addition of various amounts of $HAuCl_4 \cdot 4H_2O$ to the Au seed solution. Here, we define $[Au]_0$ as an initial concentration of $HAuCl_4 \cdot 4H_2O$ used for Au seeds in the first step, and $[Au]_1$ as a concentration of $HAuCl_4 \cdot 4H_2O$ in the second step. Then, the $[Au]_1/[Au]_0$ molar ratios used in this study corresponded to 1–9. The solutions were heated again by MW irradiation for 3 min.

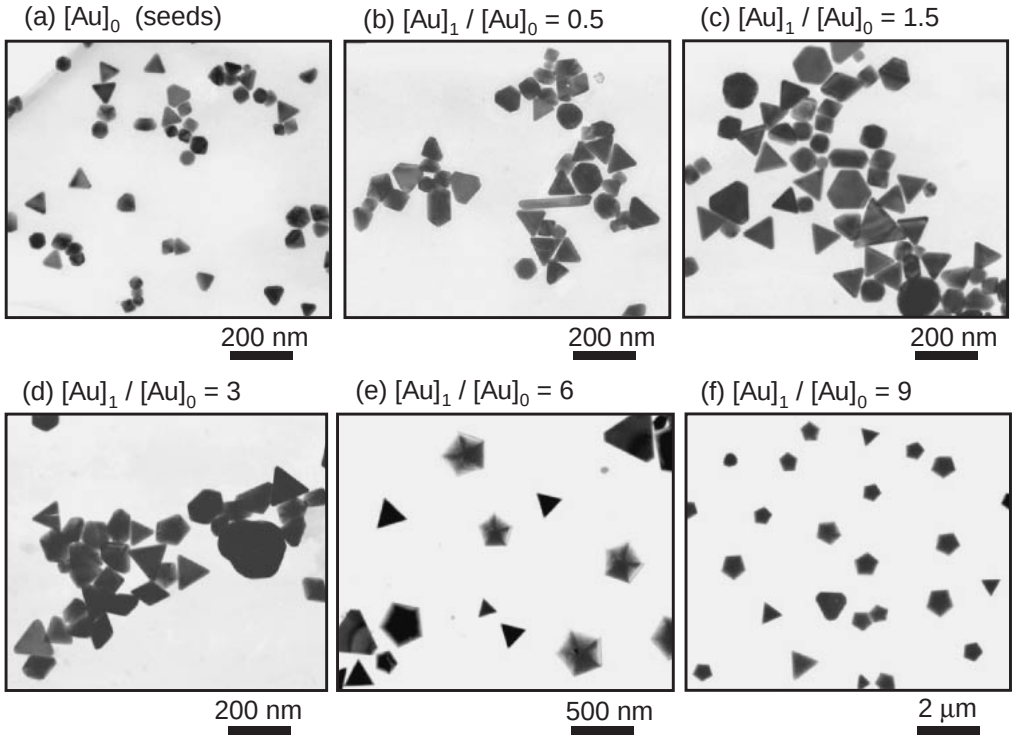

Fig. 1. TEM images of Au nanoparticles prepared from the Au(seeds)/$AuCl_4^-$/Cl^- (3.3 mM)/PVP/EG system at various $[Au]_1/[Au]_0$ molar ratios.

Procedure (2). This procedure was used for the study of effects of Cl^- anions on the Au seeds. Au(seeds)/Cl^- (3.3–51 mM)/PVP/EG solutions were prepared by the addition of various amounts of NaCl to the Au seed solution. They were heated again by MW irradiation for 3 min.

Procedure (3). This procedure was used for the study of effects of $AuCl_4^- + Cl^-$ on the Au seeds. Two kinds of experiments were carried out. In the first experiment, various amounts of NaCl was added to the Au(seeds)/$AuCl_4^-$/Cl^- (3.3 mM)/PVP/EG solution at a constant $[Au_1]/[Au]_0$ molar ratio of 3 to prepare Au(seeds)/$AuCl_4^-$/Cl^- (5.7–51 mM)/PVP/EG solutions. In the second experiment, the $[Au]_1/[Au]_0$ molar ratio in the Au(seeds)/$AuCl_4^-$/Cl^- (32 mM)/PVP/EG solution was varied in the range of 1–9 at a constant Cl^- concentration. These solutions were heated again by MW irradiation for 3 min.

Procedure (4). Since there were no MW shields in the oil-bath heating, changes in the color of the solutions could be observed more easily, and quick sampling of reagent solutions from outside was also easy. Therefore, not only MW heating (400 W) but also conventional oil-bath heating (500 W) was used, and color changes and TEM images were observed by sampling the reagent solutions. The oil-bath heating was used for the $AuCl_4^-$/PVP/EG and Au(seeds)/$AuCl_4^-$/Cl^-/PVP/EG solutions. It took 18 min to increase the solvent temperature from a room temperature to 198 °C.[4,10] Changes in the color and the morphology of the products were observed, when the temperature was increased from room temperature to 198 °C.

After MW irradiation or oil-bath heating, product solutions of Au nanoparticles were usually centrifuged at 13000 rpm for 60 min. The relative centrifugal force was 1700 G in the centrifugal separation. The precipitate was collected and redispersed in deionized water for JEOL JEM-2010 TEM and HITACHI S-4800 SEM observations. Specimens containing Au nanostructures were prepared by dropping the colloidal solutions on carbon-coated Cu grids in TEM measurements. Absorption spectra of product solutions were measured in the UV–vis–NIR region using a Shimadzu UV-3600 spectrometer. Original product solutions were diluted in EG by factors of 10–20 before spectral measurements.

Results and Discussion

Procedure (1), Effects of $AuCl_4^-$ Anions. Figures 1a–1f show TEM images of Au seeds and Au nanostructures obtained from Au(seeds)/$AuCl_4^-$/Cl^-/PVP/EG solutions in the $[Au]_1/[Au]_0$ molar ratios of 1–9. The Au seeds, shown in Fig. 1a, consist of a mixture of spherical, triangular, octahedral, decahedral, and 1-D nanoparticles with average sizes of 40–50 nm. It should be noted that significant changes in the shapes and the sizes of the Au nanostructures were observed by changing the $[Au]_1/[Au]_0$ molar ratio (Figs. 1b–1f). For example, large decahedral and triangular particles with average sizes of ≈500 nm were preferentially produced at the highest $[Au]_1/[Au]_0$ molar ratio of 9. Figures 2a and 2b show the dependence of shape and size distributions of each product on the $[Au]_1/[Au]_0$ molar ratio. The average size of spherical particles was measured by their diameters, whereas those of other particles were measured by diameters or edge lengths shown in Fig. S1 (Supporting Information). Significant changes in the shape and size distributions were found below and above the $[Au]_1/[Au]_0$ molar ratio of 4. Below the $[Au]_1/[Au]_0$ molar ratio of 4, changes in shape distributions were relatively small, whereas they were large above 4. Above the molar ratio of 4, the dominant products were triangular, hexagonal, and decahedral particles, and no spherical and octahedral particles formed. The yields of triangular and

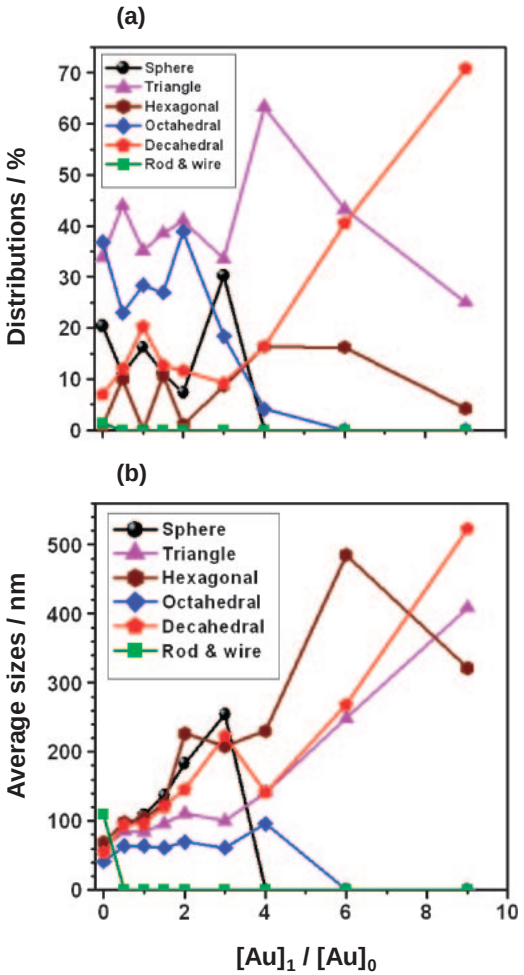

Fig. 2. Dependence of shape and size distributions of Au nanoparticles prepared from the Au(seeds)/$AuCl_4^-$/Cl^- (3.3 mM)/PVP/EG system on the $[Au]_1/[Au]_0$ ratio.

hexagonal particles had peaks in the $[Au]_1/[Au]_0$ molar ratio range of 4–6. The average size of spherical particles increases in the $[Au]_1/[Au]_0$ molar ratio range of 0–3. The size of octahedral particles, which are observed in the low $[Au]_1/[Au]_0$ molar ratio range of 0–4, is nearly constant (65 ± 16 nm). The sizes of triangular, hexagonal, and decahedral particles increased significantly with an increase in the $[Au]_1/[Au]_0$ molar ratio, though the size of hexagon decreased in the molar ratio range of 6–8. The degrees of the size increases were especially pronounced for triangular and decahedral particles above the $[Au]_1/[Au]_0$ molar ratio of 4. The average sizes of triangular, hexagonal, and decahedral particles at the highest molar ratio of 9 were larger than those of Au seeds by factors of 6.7, 6.6, and 9.7, respectively. In this experiment, large decahedral particles with an average diameter of ≈500 nm were prepared in high yield (about 70%). Sánchez-Iglesias et al.[19] have recently succeeded in the preparation of decahedral Au nanoparticles in high yield (80–90%) by using a seeded medium growth technique in *N*,*N*-dimethylformamide at ≈100 °C using ultrasonic irradiation for 60 min. They use smaller Au seeds (2–3 nm) than those used in this study (40–50 nm). They report a maximum size of decahedral particles of ≈100 nm, which is smaller than that obtained in this work

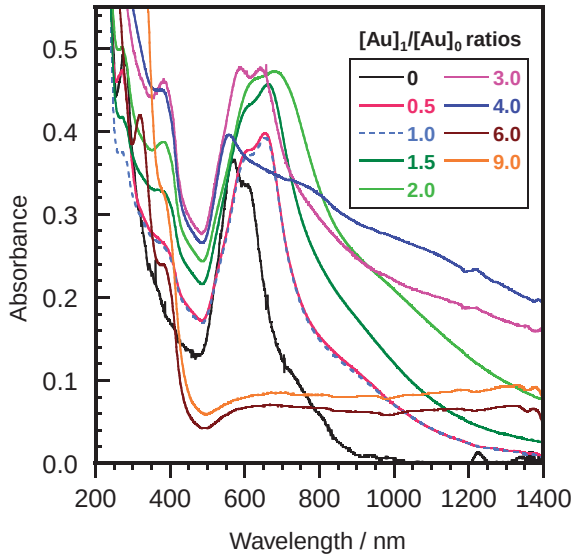

Fig. 3. UV–vis–NIR spectra of products obtained from the Au(seeds)/$AuCl_4^-$/Cl^- (3.3 mM)/PVP/EG system at various $[Au]_1/[Au]_0$ ratios.

by a factor of 5. An advantage of this study is that larger decahedral Au nanoparticles can be prepared preferentially only in three minutes under MW irradiation. To the best of our knowledge, the largest sizes of decahedral Au nanoparticles could be prepared by using Au(seeds)/$AuCl_4^-$/Cl^-/PVP/EG solutions under MW heating.

In the case of Ag nanostructures, some shapes have been prepared at high yields in the presence of halogen anions, such as Cl^-, NO_3^-, and Fe_3^+ due to selective oxidative etching of Ag particles.[16] In general, Au particles are more resistant to oxidative etching than Ag ones are. However, it has recently been found that $AuCl_4^-$ and Cl^- anions oxidatively etch Au nanoparticles in the presence of CTAB and CN^- anions.[17,18] The present data, shown in Figs. 1 and 2, suggest that either oxidative etching of Au seeds also occurs in the $AuCl_4^-$/Cl^-/PVP/EG solutions under MW heating or morphology changes take place in the present system. Why such significant changes in shapes and sizes of Au nanoparticles occur at the $[Au]_1/[Au]_0$ molar ratio of 4 will be discussed later by using more experimental data, including changes in colors and absorption spectra of various Au seed solutions with an increase in the solution temperature.

To obtain information on optical properties of Au nanostructures, absorption spectra of product solutions in procedures (1) were measured in the UV–vis–NIR region (Fig. 3). It is known that the observed wavelengths and absorbance of surface plasmon resonance (SPR) bands depend on their shapes and sizes of metallic nanoparticles. When isotropic spherical Au particles are prepared, symmetrical single SPR bands of Au nanoparticles are observed in the 500–700 nm region with a peak at ≈570 nm.[9,20–22] It is well-known that SPR bands of anisotropic oblate, platelet, prism, and 1-D products deviate from a single-peak feature and split into two or more peaks due to in- and out-of-plane plasmon resonance.[9,21,22] In Fig. 3, SPR band with two peaks at ≈570 and ≈600 nm became strong and broad with an increase in

the $[Au]_1/[Au]_0$ molar ratio from 0 to 2 due to an increase in the sizes of anisotropic Au nanoparticles. The ≈570 and ≈600 nm SPR peaks shifted to ≈600 and ≈680 nm, respectively, and the relative intensity of the ≈600 nm peak to that of the ≈570 nm peak became stronger in the same $[Au]_1/[Au]_0$ molar ratio range. At a $[Au]_1/[Au]_0$ molar ratio of 3, the SPR peaks blue shifted and became broad. At a $[Au]_1/[Au]_0$ molar ratio of 4, the SPR peak shifted to ≈550 nm with a single peak having a long tail band in the vis–NIR region. These significant spectral changes are consistent with the shape and size changes in the TEM images of products below and above a molar ratio of 4. At the high $[Au]_1/[Au]_0$ molar ratios of 6–9, only weak broad bands due to reflection of large anisotropic products were observed.

Procedure (2), Effects of Cl^-. To obtain further information on roles of Cl^- for Au seeds, Au nanoparticles were prepared through procedure (2). Figure S2 (Supporting Information) shows TEM images obtained from the Au(seeds)/Cl^- (0–48 mM)/PVP (1 M)/EG system under MW irradiation for 3 min. Figures S3 and S4 (Supporting Information) show shape distributions and UV–vis–NIR spectra obtained at various Cl^- concentrations. No significant changes were observed in the shapes and the sizes of the products, and small changes in UV–vis–NIR spectra were observed upon the addition of NaCl. On the basis of these facts, it was concluded that Cl^- anions scarcely etch Au seeds in EG below 198 °C without the presence of $AuCl_4^-$ anions.

Procedure (3), Effects of $AuCl_4^-$ + Cl^-. In procedure (1), significant shape and size changes were observed upon the addition of $AuCl_4^-$ anions to the Au seed solutions, whereas little changes were found after the addition of Cl^- anions to Au seeds in procedure (2). To obtain information on the addition effects of Cl^- anions in the presence of $AuCl_4^-$, Au nanoparticles were prepared through procedure (3). Figure 4 shows typical TEM images of product Au nanoparticles obtained from the Au(seeds)/$AuCl_4^-$/Cl^- (3.3–51 mM)/PVP (1 M)/EG system at a $[Au]_1/[Au]_0$ molar ratio of 3. At a Cl^- concentrations of 3.3 mM, a mixture of spherical, triangular, and octahedral particles formed. At Cl^- concentrations of 13 and 32 mM, besides small amounts of triangular and decahedron particles observed in procedure (1), icosahedral particles with uniform sizes formed preferentially, and the yields of spherical and octahedral particles greatly decrease. At the highest Cl^- concentration of 51 mM, the yield of icosahedral particle became small, and larger spherical, triangular, and decahedral particles were the dominant products.

In order to obtain definite information on shapes of Au nanoparticles, SEM images were observed at a Cl^- concentration of 32 mM. Figure 5a shows a typical SEM image of a mixture of various shapes of particles. Figures 5b–5g show typical triangular, hexagonal, octahedral, decahedral, icosahedral, and 1-D products, respectively. The TEM-SAED pattern of icosahedral particle was also measured (Fig. S5 (Supporting Information)), and a typical hexagonal pattern for icosahedral particles was observed, which is consistent with the predicted pattern.[23] On the basis of the TEM, TEM-SAED, and SEM data, it is clearly demonstrated that octahedral particle is single crystal, triangular and hexagonal plates consist of single-twin particles (STP), decahedral and icosahedral particles are multiple-twin particles (MTP), respectively (Fig. 6). It was found that spherical particles were quasi-spherical polycrystals having many facets from SEM images and minor 1-D products were ribbon-like plate having {111} facets on the top and down plates. In Fig. 6 are summarized the crystal structures of each product and their growth mechanisms on the basis of growth mechanisms of such FCC crystals as Au and Ag.[24–28]

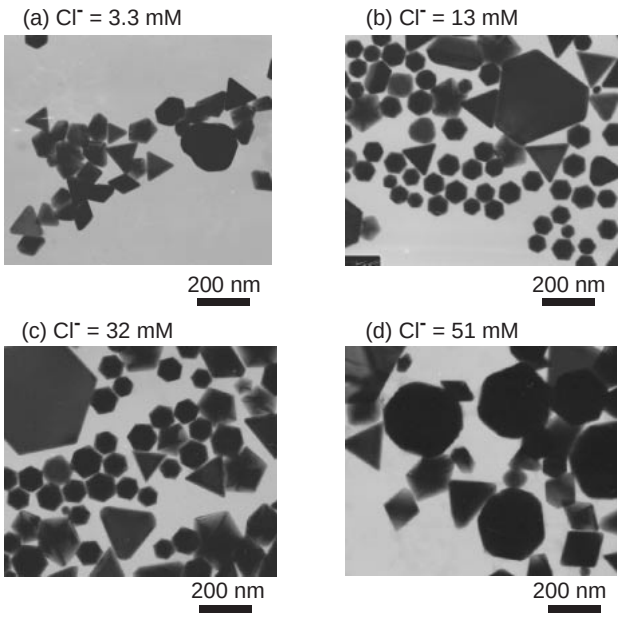

Fig. 4. TEM images of Au nanoparticles prepared from the Au(seeds)/$AuCl_4^-$/Cl^- (3.3–51 mM)/PVP/EG system at a constant $[Au]_1/[Au]_0$ molar ratio of 3.

Figures 7a–7f show TEM images of Au nanostructures obtained from the Au(seeds)/$AuCl_4^-$/Cl^- (32 mM)/PVP/EG system at $[Au]_1/[Au]_0$ ratios of 1–9. Although the yield of icosahedral particles was very small in the low $[Au]_1/[Au]_0$ ratio range of 1–2, it increased rapidly at $[Au]_1/[Au]_0$ ratios above 3. In Figs. 8a and 8b are summarized the dependence of shape and size distributions of each product on the Cl^- concentration and the $[Au]_1/[Au]_0$ ratio under the experimental conditions shown in Figs. 4 and 7, respectively. The addition of Cl^- anions caused the yield of icosahedral particles to increase, whereas those of the other particles decreased. The yield of icosahedral particles had a maximum at a Cl^- concentration of 13 mM (Fig. 8a-1) and at a $[Au]_1/[Au]_0$ ratio of 4 (Fig. 8a-2). The size of triangular particle increased with an increase in the Cl^- concentration, whereas no significant changes in sizes are observed for octahedral and icosahedral particles (Fig. 8b-1). The sizes of spherical, hexagonal, and decahedral particles decreased in the concentration range of 3.3–13 mM range and then increased in the range of 13–51 mM (Fig. 8b-1). Sizes of the particles had a maximum in the $[Au]_1/[Au]_0$ ratio range of 2–6, and they were small at a $[Au]_1/[Au]_0$ ratio of 1 and a $[Au]_1/[Au]_0$ ratio of 9 (Fig. 8b-2).

Figures 9a and 9b show UV–vis–NIR absorption spectra of Au products, shown in Figs. 4 and 7, respectively. In Fig. 9a, the SPR band of Au seeds with a peak at ≈550 nm became

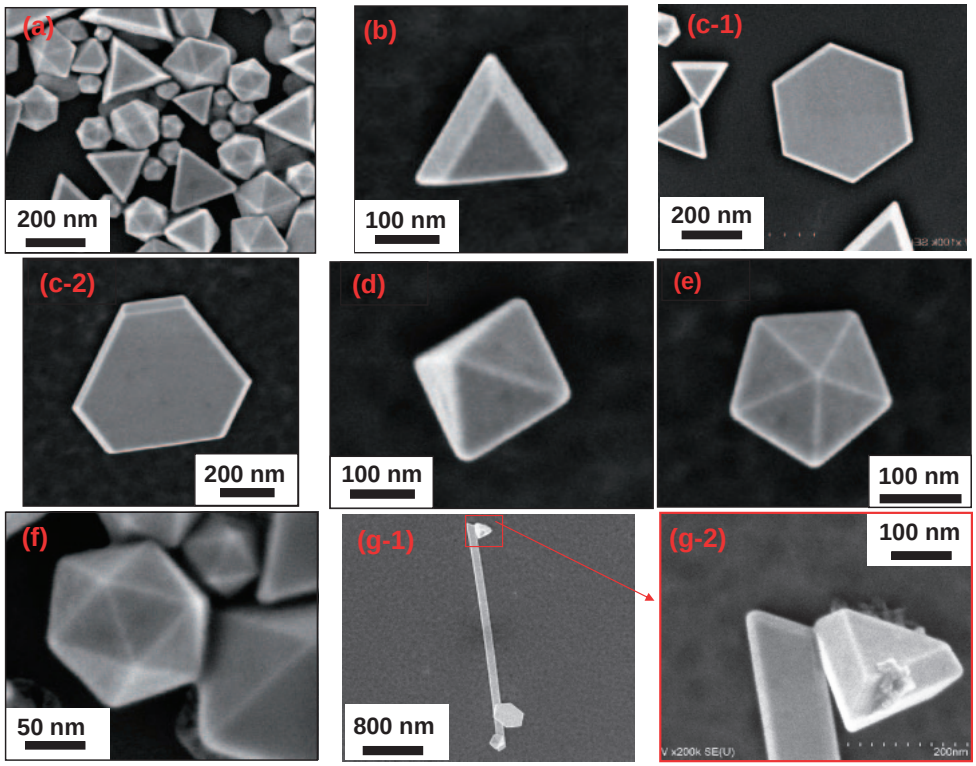

Fig. 5. SEM images of Au nanoparticles prepared from the Au(seeds)/$AuCl_4^-$/Cl^- (32 mM)/PVP/EG system at a $[Au]_1/[Au]_0$ molar ratio of 3.

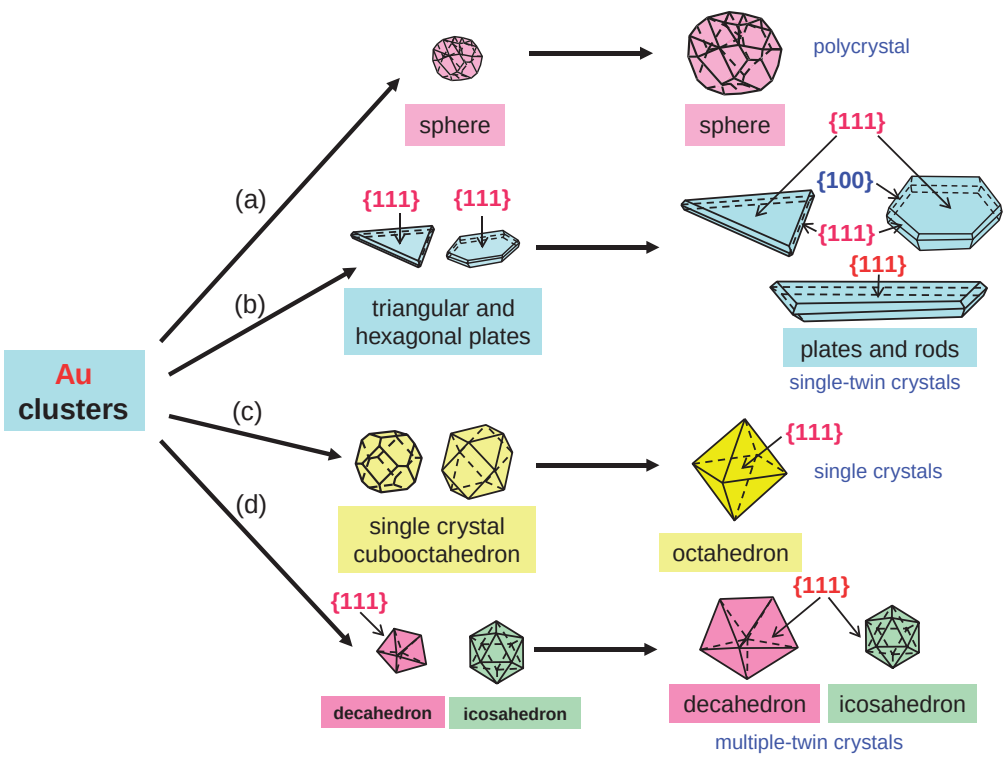

Fig. 6. Crystal structures and their growth mechanisms of Au nanosparticles prepared from the Au(seeds)/$AuCl_4^-$/Cl^-/PVP/EG system.

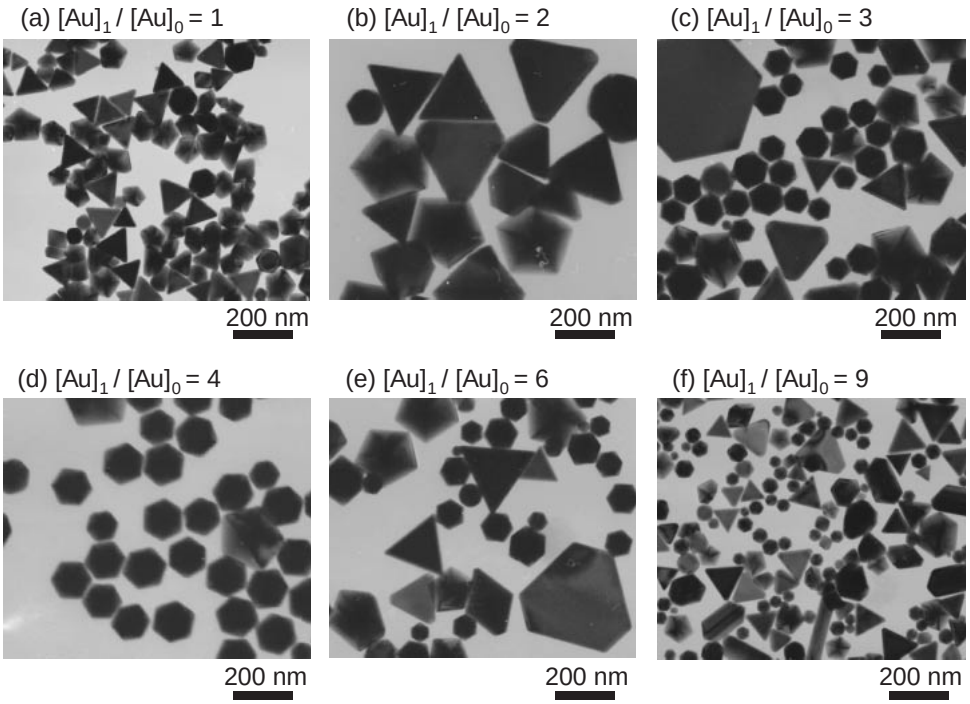

Fig. 7. TEM images of Au nanoparticles prepared from the Au(seeds)/$AuCl_4^-$/Cl^- (32 mM)/PVP/EG system at various $[Au]_1/[Au]_0$ molar ratios.

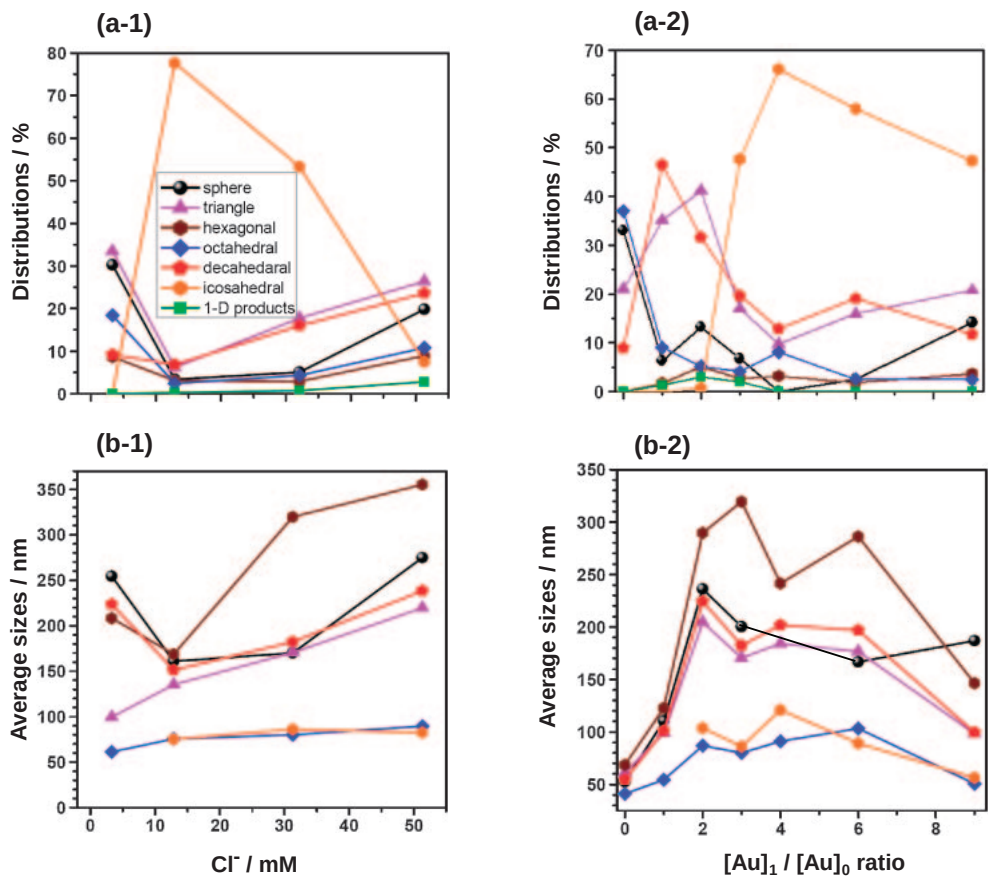

Fig. 8. (a1) and (b1): Dependence of shape and size distributions of Au nanoparticles prepared from the Au(seeds)/$AuCl_4^-$/Cl^- (3.3–51 mM)/PVP/EG system at a constant $[Au]_1/[Au]_0$ molar ratio of 3. (a2) and (b2): Dependence of shape and size distributions of Au nanoparticles prepared from the Au(seeds)/$AuCl_4^-$/Cl^- (32 mM)/PVP/EG system at various $[Au]_1/[Au]_0$ molar ratios.

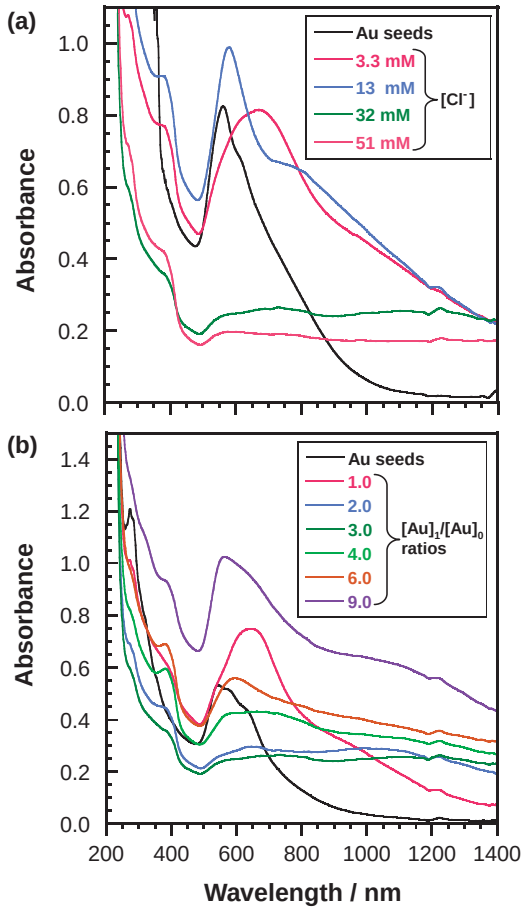

Fig. 9. UV–vis–NIR absorption spectra of Au nanoparticles (a) prepared from the Au(seeds)/$AuCl_4^-$/Cl^- (3.3–51 mM)/PVP/EG system at a constant $[Au]_1/[Au]_0$ molar ratio of 3 and (b) prepared from the Au(seeds)/$AuCl_4^-$/Cl^- (32 mM)/PVP/EG system at various $[Au]_1/[Au]_0$ molar ratios.

broad and shifted to ≈660 nm at a Cl^- concentration of 3.3 mM. It became stronger and shifted again to ≈570 nm at a Cl^- concentration of 13 mM. The peak became weak and broad at Cl^- concentrations of 32 and 51 mM. One reason for this is the formation of large aggregated particles due to salting-out of Au nanoparticles at high Cl^- concentrations. In Fig. 9b, the SPR band of Au seeds became strong, and the peak at ≈540 nm shifted to ≈640 nm at a $[Au]_1/[Au]_0$ ratio of 1. At $[Au]_1/[Au]_0$ ratios of 2 and 3, the SPR bands became very weak probably due to salting-out. However, with an increase in the $[Au]_1/[Au]_0$ ratio from 4 to 9, the SPR band with a long tail band became strong again due to a decrease in sizes of Au nanoparticles in this range. The peak of SPR band at the highest ratio of 9 was observed at ≈570 nm, which is similar to that of Au seed solution.

Changes in Colors of Solutions and Absorption Spectra [Procedure (4)]. In this study, we studied the shape- and size-controlled synthesis of Au nanocrystals in the presence of Au seeds. It was found that the shapes and the sizes of Au nanocrystals depended significantly on the concentrations of $AuCl_4^-$ and Cl^- anions. To obtain more information on the mechanism of shape and size changes of Au nanostructures in the present system, colors of reagent and product solutions and their UV–vis–NIR absorption spectra were measured at various conditions using both MW and oil-bath heating. Figure 10a shows the colors and UV–vis absorption spectra of $AuCl_4^-$ (2.4 mM)/PVP (1 M)/EG solutions obtained at various temperatures under MW heating. The solution color before MW heating (20 °C) was yellow and transparent. The yellow color became light in the range of 70–145 °C and colorless at 155 °C. The UV–vis spectrum before MW heating, shown in Fig. 10b, had of a single symmetric band for $AuCl_4^-$ complex anion in the 280–380 nm region with a peak at ≈322 nm. This peak became weak with an increase in the solution temperature and almost disappeared at 155 °C. The color of solution at 160 °C was similar to that at 155 °C. After the solution temperature was increased above 160 °C, the solution became red and brown due to the formation of Au nanoparticles, as shown in Fig. 10a at 168 and 198 °C. These results suggest that the reduction of $AuCl_4^-$ anion to $AuCl_2^-$ + 2Cl (or Cl_2) starts at about 70 °C and further reduction of $AuCl_2^-$ to $Au^0 + Cl^- + Cl$ occurs above ≈160 °C:

$$AuCl_4^- \rightarrow AuCl_2^- + 2Cl \text{ (or } Cl_2), \quad (3)$$

$$AuCl_2^- \rightarrow Au^0 + Cl^- + Cl. \quad (4)$$

When EG was used as a solvent and a reductant, Au particles are produced by the following two step reaction sequence:[4]

$$CH_2OH\text{–}CH_2OH \rightarrow CH_3CHO + H_2O, \quad (5a)$$

$$6CH_3CHO + 2Au^{3+} \rightarrow 2Au + 6H^+ + 3CH_3COCOCH_3. \quad (5b)$$

However, we think that, besides the second reaction (5b), the following reaction must occur above ≈160 °C in the present experiments, because Au^{3+} is partly reduced to Au^+ via process (3) before ≈160 °C:

$$2CH_3CHO + 2Au^+ \rightarrow 2Au + 2H^+ + CH_3COCOCH_3. \quad (5c)$$

Figures 11a and 11b show color changes of solutions of the Au(seeds)/$AuCl_4^-$/Cl^- (3.3 mM)/PVP/EG and Au(seeds)/$AuCl_4^-$/Cl^- (32 mM)/PVP/EG systems at a $[Au]_1/[Au]_0$ ratio of 6 under the oil-bath heating, respectively. In Fig. 11a, the brown Au seed solution became light in the range of 80–100 °C. The color changed to red in the range of 110–165 °C and dark brown again at 198 °C, due to the formation of Au nanoparticles in the range of 165–198 °C. On the other hand, more dramatic changes in colors of solutions were observed at a Cl^- concentration of 32 mM after adding NaCl, as shown in Fig. 11b. The brown Au seed solution became light at 60 °C and became red, pale red, and orange in the range of 80–110 °C. It should be noted that the color became yellow and transparent at 120 °C, which are the same as that of the original solution of $AuCl_4^-$ (2.4 mM)/PVP (1 M)/EG solution (Fig. 10a). The yellow color became light and colorless at 162 °C, as observed for the original solution of $AuCl_4^-$ (2.4 mM)/PVP (1 M)/EG solution at 155 °C (Fig. 10a). At 198 °C, a brown solution was obtained due to the formation of Au nanoparticles above 162 °C.

Figures 11c and 11d show UV–vis–NIR spectra of solutions of Figs. 11a and 11b, respectively, at various temperatures. The absorption spectrum of the Au seed solution had an asymmetric SPR band for anisotropic Au nanoparticles with

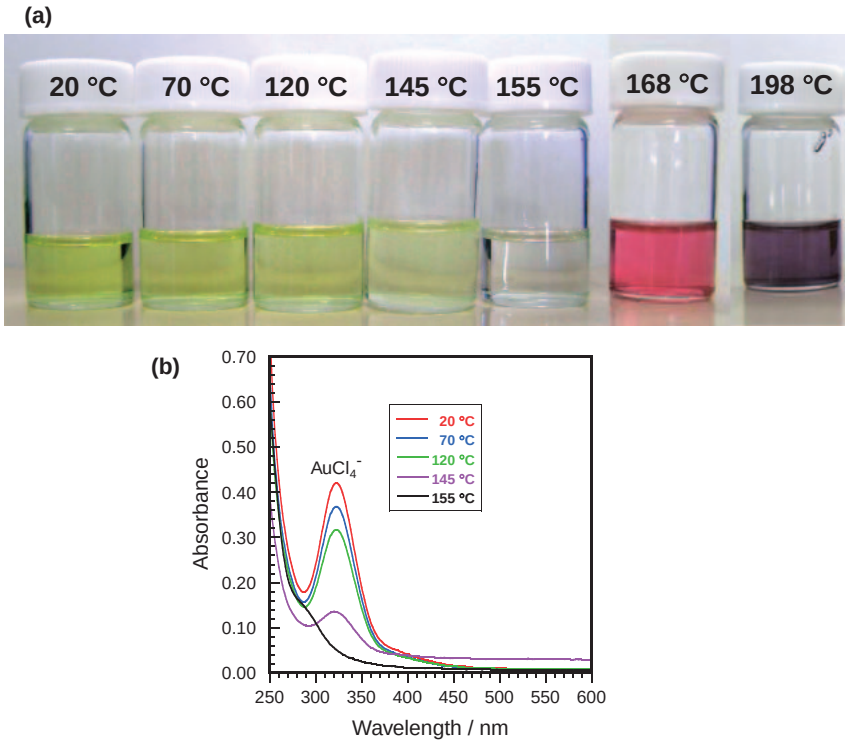

Fig. 10. (a) Colors and (b) UV–vis spectra of the $AuCl_4^-$ (2.4 mM)/PVP (1 M)/EG system at various temperatures under MW heating. Colors of original solutions were observed in (a), while spectra (b) were observed by diluting original solutions in EG by a factor of 20.

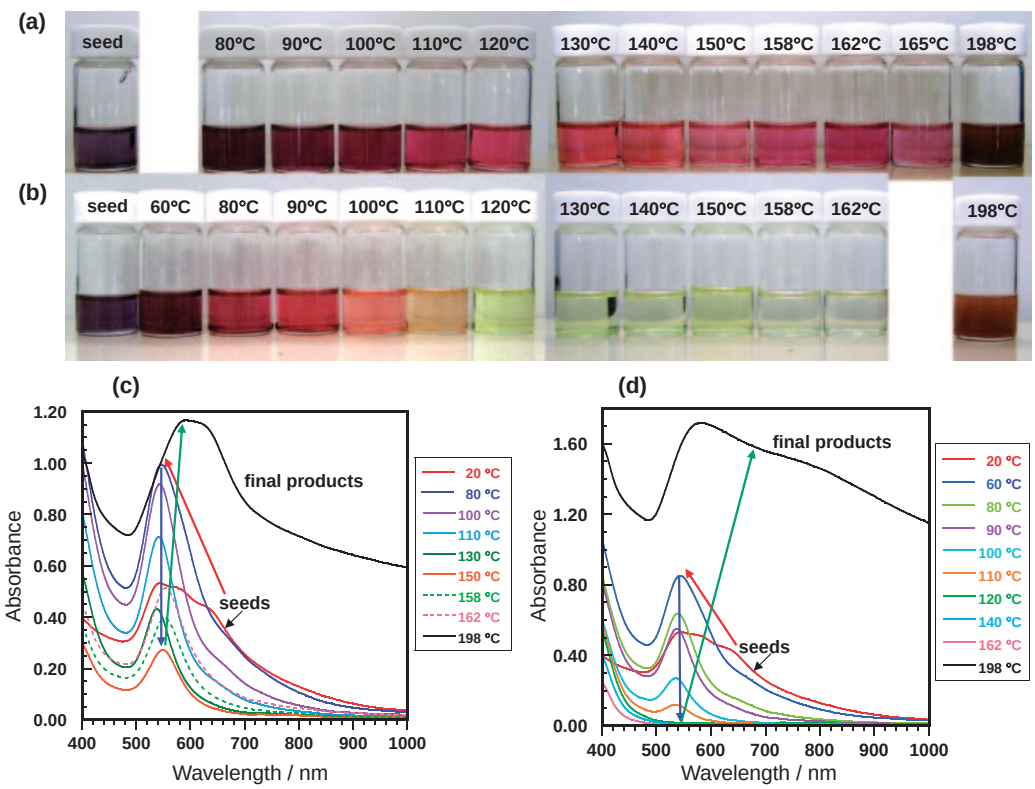

Fig. 11. Colors of solutions of (a) the Au(seeds)/$AuCl_4^-$/Cl^- (3.3 mM)/PVP/EG system and (b) Au(seeds)/$AuCl_4^-$/Cl^- (32 mM)/PVP/EG system at a $[Au]_1/[Au]_0$ molar ratio of 6 at various temperatures under oil-bath heating (500 W). (c) and (d): UV–vis–NIR spectra of solutions shown in (a) and (c), respectively. Colors and absorption spectra were measured by diluting original solutions by a factor of 10.

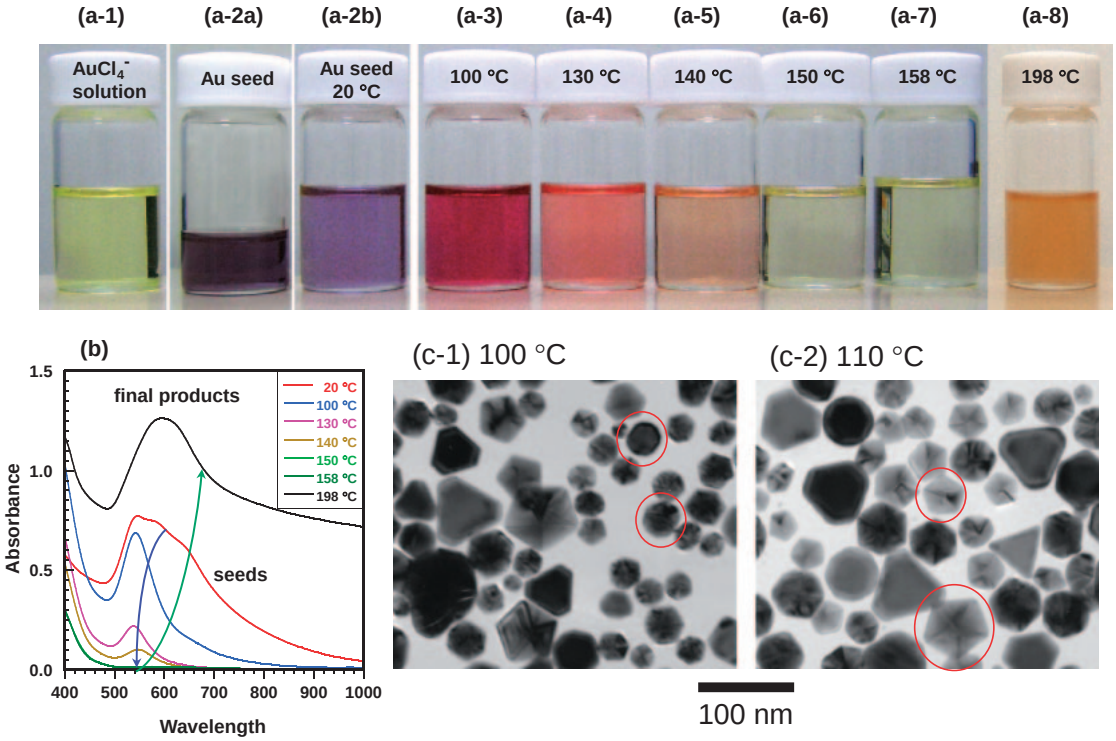

Fig. 12. (a) Colors of solutions and (b) UV–vis–NIR spectra of the Au(seeds)/$AuCl_4^-$/Cl^- (3.3 mM)/PVP/EG system at a $[Au]_1/[Au]_0$ molar ratio of 9 at various temperatures under oil-bath heating (500 W). (c) TEM images of Au nanoparticles obtained at 100 and 110 °C. Colors and absorption spectra in (a) and (b) were measured by diluting original solutions in EG by a factor of 10 except for (a2) and (a2-a), which were original solutions and (a2-b) which was diluted in EG by a factor of 20. Typical quasi-spherical and decahedral particles are surrounded by red circles in (c-1) and (c-2).

a peak at ≈540 nm. In Fig. 11c, at 80 °C, the asymmetric peak changed to a symmetric one at the same wavelength, which is similar to the SPR band of spherical Au nanoparticles. The increase in the absorbance in the temperature range of 80–110 °C is explained by larger absorption coefficients of isotropic spherical nanoparticles than those of anisotropic seeds. The symmetric SPR band with a single peak at ≈540 nm became further weak in the temperature range of 130–150 °C due to oxidative etching, and became strong and shifted to red in the temperature range of 150–198 °C due to crystal growth. In Fig. 11d, the asymmetric peak for Au seeds also changed to a symmetric one at a low temperature of 60 °C. With an increase in the solution temperature from 60 to 110 °C, the symmetric band at ≈540 nm became weak and disappeared in the range of 120–162 °C. In both Figs. 11c and 11d, a strong SPR band with a tail band in the longer wavelength region was observed at 198 °C, due to the formation of large particles having spherical shape or less sharp edges than those obtained by MW heating in the range of 162–198 °C. The above results at a $[Au]_1/[Au]_0$ ratio of 6 indicates that Au seeds are etched to small isotropic particles in the range of 80–165 °C range for the Au(seeds)/$AuCl_4^-$/Cl^- (3.3 mM)/PVP/EG system, whereas Au seeds are more rapidly etched and converted to ultrafine Au nanoparticles (diameter < 2 nm), Au clusters, and $AuCl_n^-$ ($n = 4$ and 2) anions in the range of 120–162 °C for the Au(seeds)/$AuCl_4^-$/Cl^- (32 mM)/PVP/EG system. The change in the color from yellow to transparent in the range of 120–162 °C indicates that the reduction of $AuCl_4^-$ to $AuCl_2^-$ occurs in this temperature range.

The effects of the Cl^- concentration were studied in Fig. 11 at a constant $[Au]_1/[Au]_0$ ratio of 6. We also examined the effects of the $[Au]_1/[Au]_0$ ratio under the oil-bath heating. Figure 12a shows the color changes of the Au(seeds)/$AuCl_4^-$/Cl^- (3.3 mM)/PVP/EG solution at the highest $[Au]_1/[Au]_0$ ratio of 9. It should be noted that brown solution changes to red in the 100–130 °C range, orange at 140 °C, and light yellow and transparent in the 150–158 °C range, and finally orange solution was obtained at 198 °C. The UV–vis–NIR absorption spectra are shown in Fig. 12b. These spectral changes are similar to those observed in the Au(seeds)/$AuCl_4^-$/Cl^- (32 mM)/PVP/EG system at a $[Au]_1/[Au]_0$ ratio of 6 (Fig. 11b). Thus, it was concluded that oxidative etching of Au seeds to ultrafine Au nanoparticles (diameter < 2 nm), Au clusters, and $AuCl_n^-$ ($n = 4$ and 2) also occurs in the 150–158 °C range at a high $[Au]_1/[Au]_0$ ratio of 9.

Figure 12c show TEM images of Au nanoparticles obtained at 100 and 110 °C. Many quasi-spherical particles were observed at 100 °C, due to oxidative etching of anisotropic particles by the $AuCl_4^-$ + Cl^- anions. It should be noted that such quasi-spherical particles disappeared at 110 °C and a large amount of decahedral particles appeared. This result suggests that either spherical particles are more rapidly etched than the decahedral particles or some quasi-spherical particles change to decahedral particles in this temperature range. Au seed solutions became yellow as in the case of original $AuCl_4^-$ (2.4 mM)/PVP (1 M)/EG solution in the range of 150–158 °C

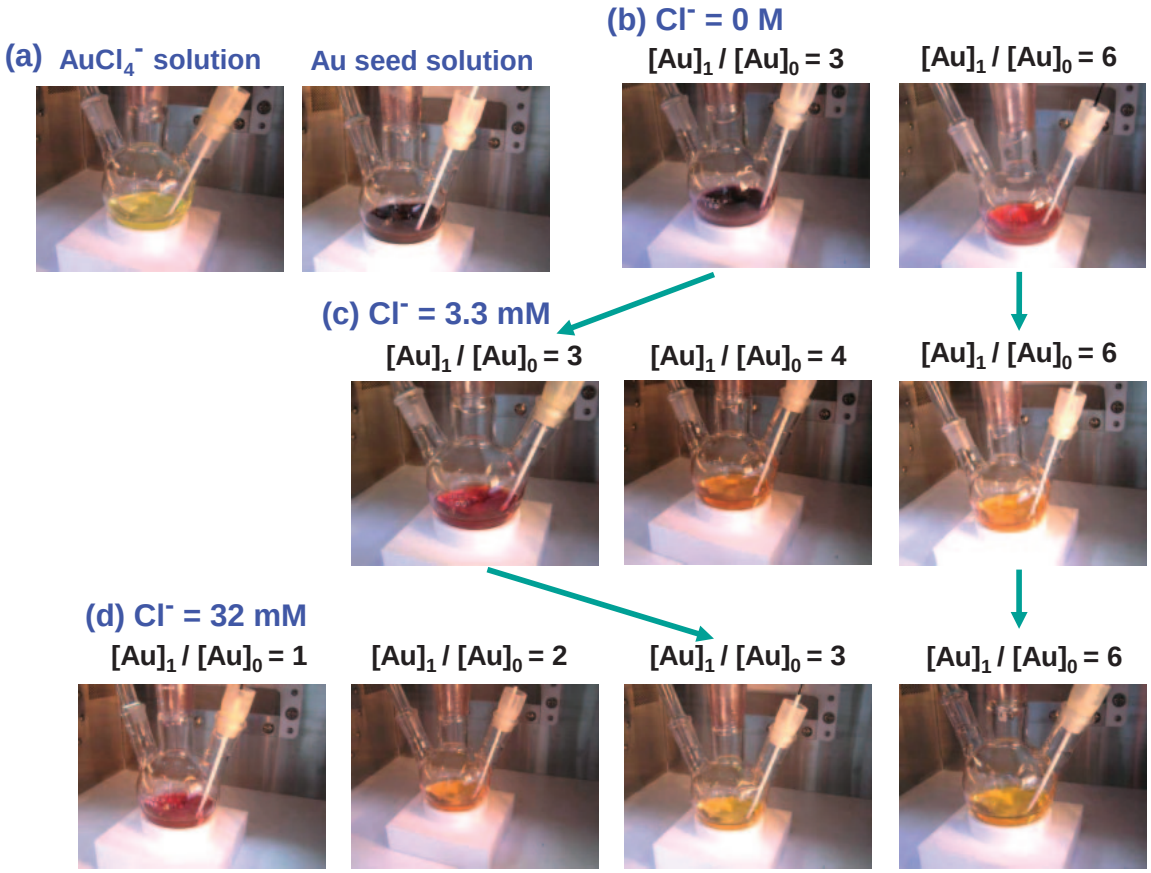

Fig. 13. (a) $AuCl_4^-$ (2.4 mM)/PVP (1 M)/EG solution before heating and Au(seeds)/Cl^- (3.3 mM)/PVP/EG solution prepared under the standard condition. (b)–(d) color of solutions for the Au(seeds)/$AuCl_4^-$/PVP/EG system under MW heating at 160 °C at various Cl^- concentrations and $[Au]_1/[Au]_0$ molar ratios. Colors were measured by diluting original solutions in EG by a factor of 10.

range, indicating that all Au seeds are etched and dissolved as ultrafine Au nanoparticles (diameter < 2 nm), Au clusters, and $AuCl_n^-$ ($n = 4$ and 2) anions in this temperature.

It is known that the intensity of SPR bands of spherical Au nanoparticles decreases with decreasing diameter from 100 to 5 nm and almost disappears below about 2 nm. This means that there is a possibility that small Au nanoparticles less than 2 nm remain in the yellow solutions. It was difficult to observe TEM images of Au nanoparticles, because such small Au nanoparticles could not be separated by using centrifugal separation. In addition, the boiling point of EG (198 °C) was too high to dry the product solution on TEM grids. In order to examine whether small nanoparticles were really involved or not in yellow solution after oil-bath heating in water below 100 °C, TEM images of yellow solutions were observed.[29] Since the boiling point of water is 100 °C, it could be dried by leaving a drop of product solution on the TEM grids overnight. We could observe small Au nanoparticles with average diameters of 2–3 nm from the yellow solutions in the Au(seeds)/$AuCl_4^-$ (14.4 mM)/Cl^- (38.4 mM)/PVP/H_2O system, even though no SPR bands were observed due to oxidative etching by $AuCl_4^-$ + Cl^- anions. On the basis of this finding, small Au nanoparticles (<3 nm) may also remain in yellow EG solution in many cases. The small particles act as nucleation seeds in the forthcoming reduction of metallic ions at higher temperatures.

Finally, effects of MW irradiation were studied by observing the changes in the color of reagent solutions. Figure 13a shows original yellow and transparent $AuCl_4^-$ (2.4 mM)/PVP (1 M)/EG solution and brown Au(seeds)/Cl^- (3.3 mM)/PVP (1 M)/EG solution before MW heating. Figures 13b–13d show colors of Au(seeds)/$AuCl_4^-$/Cl^-/PVP/EG solutions with Cl^- concentrations of 0, 3.3, and 32 mM, respectively, at 160 °C and various $[Au]_1/[Au]_0$ ratios. Although there was little color change at a $[Au]_1/[Au]_0$ ratio of 3 in Fig. 13b, the solution became red at a $[Au]_1/[Au]_0$ ratio of 6. This suggests that $AuCl_4^-$ alone has a weak ability to etch Au seeds. As shown in Fig. 10, $AuCl_4^-$ anions decomposed preferentially leading to Cl^- ions in the solution temperature range of 70–160 °C. This result indicates that Cl^- anions are produced in the presence of $AuCl_4^-$ anions through decomposition below ≈160 °C, even if there are no Cl^- anions in the initial Au seed solution at 20 °C. Thus, $AuCl_4^-$ and Cl^- resulting from $HAuCl_4$ contribute to the etching of Au seeds in Fig. 13b. In Fig. 13c, 3.3 mM of Cl^- anions were initially involved in the solutions through the first process for the preparation of the Au seeds. In such a condition, the colors of the solutions at $[Au]_1/[Au]_0$ ratios of 3, 4, and 6 were red, orange, and yellow, respectively, at 160 °C. In the case of oil-bath heating, the color of the solution at 160 °C was red at a $[Au]_1/[Au]_0$ ratio of 6 (Fig. 11a). This shows a direct evidence that Au seeds are etched more

rapidly in the MW heating than in the oil-bath heating at the same solution temperature. At a high Cl^- concentration of 32 mM, the etching rate of Au seeds becomes fast. Therefore, the colors of solution at 160 °C were red at a low $[Au]_1/[Au]_0$ ratio of 1 and orange or yellow at high $[Au]_1/[Au]_0$ ratios of 2–6.

The effects of MW irradiation have been studied by Tanaka and Sato using frequency response analysis of metallic nanoparticles and molecular dynamics simulation of water and a dilute saline solution.[30,31] They have found that metallic nanoparticles are heated by skin effects of MW penetrated into insides of nanoparticles. The penetration depth of MW is estimated to be on the order of a few μm, which is larger than the particle size.[32] They have also found that a dilute NaCl solution is heated more significantly than pure water by MW irradiation. This is due to rapid heating of salt ions, especially that of large salt ions Cl^-, through field-induced motion by the MW electric field and energy transfer by the interactions between salt ions and water molecules. We studied effects of MW irradiation. At first, we compared the decomposition rates of $AuCl_4^-$ under MW and oil-bath heating by observing reduction of an $AuCl_4^-$ absorption peak in EG solution in the temperature range of 20–160 °C. The reduction rate of the $AuCl_4^-$ absorption peak in the oil-bath heating was similar to that in the MW heating (Fig. 10). Thus, there is no difference in the thermal decomposition rate of $AuCl_4^-$ via process (3) between the two heating methods. On the other hand, Au seeds are etched more rapidly under MW heating. One reason for the faster etching rate under MW irradiation will be MW heating of Au seeds due to the penetration of MW through Au nanoparticles. Another reason will be rapid heating of Cl^- and $AuCl_4^-$ anions by MW irradiation, which enhances the etching rate of Au seeds.

As shown above, we found that Au seeds are etched in both MW and oil-bath heating below ≈160 °C. They were partially or completely etched depending on heating methods, heating temperature, and concentrations of $AuCl_4^- + Cl^-$ ions. However, an important point is that, after heating solutions from ≈160 to 198 °C, highly crystalline polygonal particles with well-defined facets were preferentially synthesized only in MW heating. In the case of oil-bath heating, the major products obtained from the same Au seeded medium after heating at 198 °C were spherical particles or polygonal particles having less sharp edges, due to lower degree of crystallinity. Similar large spherical particles have also been obtained from the $HAuCl_4 \cdot 4H_2O$/PVP/EG system under oil-bath heating without using Au seeds.[4,10] These results led to conclusion that MW heating is necessary for the preparation of Au nanocrystals with well-defined facets. In our experiments, the formation of Au nanocrystals took place in the high temperature range of 160–198 °C. In the case of MW heating, nanoparticles will be more locally heated due to the penetration of electromagnetic wave into nano-sized metallic particles under growth. This is a major reason for the formation of Au nanocrystals with well-defined facets under MW heating.

Etching and Growth Mechanisms of Au Nanostructures. Rodríguez-Fernández et al. have recently reported that Au^0 metals are etched by $AuCl_4^- + Cl^-$ ions in the $HAuCl_4 \cdot 3H_2O/NaBH_4/CTAB/H_2O$ system:[17]

$$2Au^0 + AuCl_4^- + 2Cl^- \rightarrow 3AuCl_2^-. \quad (6)$$

Here, Cl^- anions are supplied from decomposition of $AuCl_4^-$ anions during the reduction by $NaBH_4$. They reported that reaction (6) only took place in the presence of CTAB, because of a change in the reduction potential of $AuCl_4^-$, and led to gradual oxidation of Au nanoparticles. In the present study, we found that Au seeds were etched in the Au(seeds)/$AuCl_4^-/Cl^-$/PVP/EG system under MW and oil-bath heating. We found that the oxidative etching of Au seeds occurred only in the presence of both $AuCl_4^-$ and Cl^- ions. It was therefore concluded that oxidation reaction (6) also took place in the present Au(seeds)/$AuCl_4^-/Cl^-$/PVP/EG system. Only large spherical particles were obtained without addition of PVP, as reported in our previous paper.[4] It is therefore highly likely that PVP not only acts as a protecting agent for aggregation of Au nanoparticles but also contributes to the formation of nanocrystals with well-defined facets and sharp edges by selective adsorption of PVPs on specific facets of growing crystals.

We found that the spherical particles were polycrystals, the octahedral particles were single crystals, triangular and hexagonal plate-like particles were STPs, and decahedral and icosahedral particles were MTPs. It has been known for Ag nanoparticles that MTPs are etched by Cl^-/O_2, whereas such single crystals as cubic particles are inactive for oxidative etching.[16] From our recent oxidative etching studies on Ag and Au@Ag particles by Cl^-/O_2 under MW–polyol method, a slightly different etching selectivity has been obtained.[33] In our case, spherical Ag particles were etched, and not only single cubic crystals but also triangular pyramidal STPs and decahedral MTPs were not. In the present study, it was clearly shown that different shape selective etching occurs in the case of Au nanoparticles. The etching rates of the spherical and octahedral Au nanoparticles by $AuCl_4^- + Cl^-$ anions were faster than those of single-twin and multiple-twin Au nanoparticles. Therefore, single-twin triangular plates and multiple-twin decahedral and icosahedral particles were preferentially produced.

It was found that etching rate of Au seeds depended on the concentrations of both $AuCl_4^-$ and Cl^- anions. The etching rate increased with increasing the $AuCl_4^-$ concentration. On the other hand, the etching rate of Au seeds had a maximum at a Cl^- concentration of about 10 mM, because salting-out of Au nanoparticles occurs at high NaCl concentrations. On the basis of many experiments involving Procedures (1)–(4), we found that there were three typical cases in the etching process of Au seeds by $AuCl_4^- + Cl^-$ anions below ≈160 °C and crystal growth of Au nanoparticles in the 160–198 °C range under MW heating. Two typical limited cases are shown in Fig. 14. The first limited case (case (a) in Fig. 14) involved etching of the Au seeds, which partially occurred below ≈160 °C and at low $AuCl_4^- + Cl^-$ concentrations. In this case, little change in the number of Au seeds occurs due to incomplete etching of Au seeds and the deposition of Au layers occurs over the Au seeds in the range of 160–198 °C. In such a case, major products are triangular and octahedral particles, which are the same as those involved in the Au seeds (e.g. below a $[Au]_1/[Au]_0$ ratio of 2 in Fig. 2). The second limited

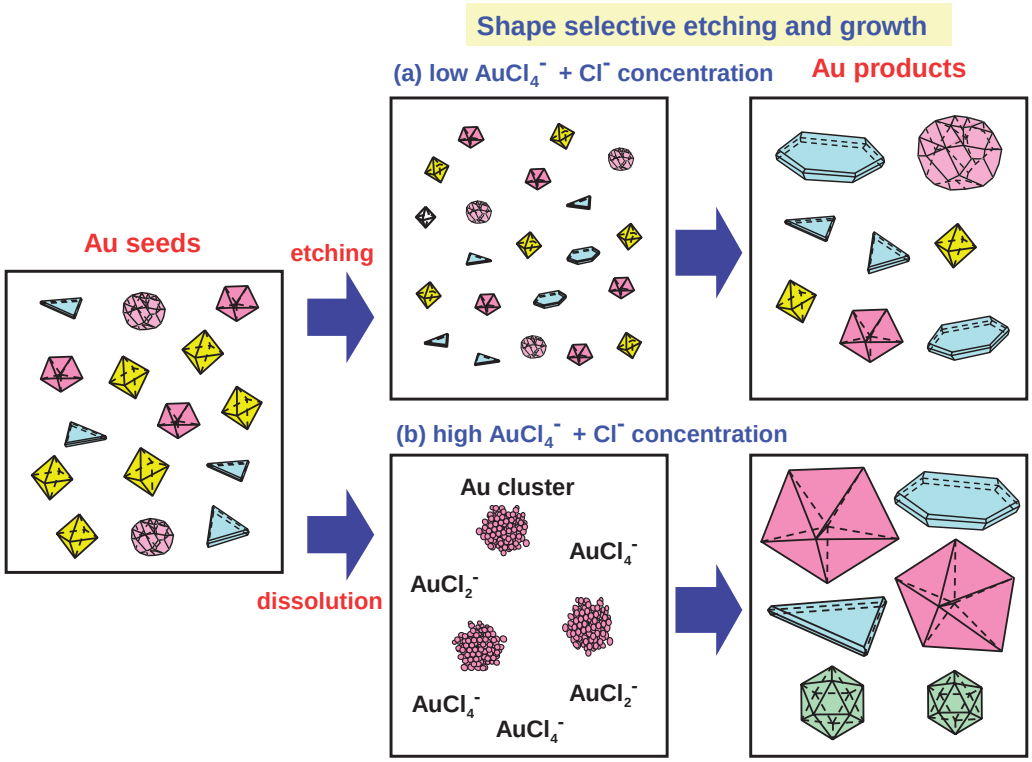

Fig. 14. Etching and crystal growth mechanism of Au nanostructures from the Au(seeds)/$AuCl_4^-$/Cl^-/PVP/EG system.

case (case (b) in Fig. 14) is that Au seeds are completely etched by $AuCl_4^-$ + Cl^- anions until ≈160 °C (e.g. above $[Au]_1/[Au]_0$ ratios of 4 in Fig. 2). In this case, the shapes and sizes of product particles are determined from shapes of new Au seeds, the formation of which is favorable under the new given conditions. The third case is an intermediate case between the above two cases (e.g. $[Au]_1/[Au]_0$ ratios of 2–4 in Fig. 2). In this case, spherical particles are partially dissolved at $[Au]_1/[Au]_0$ ratios of 3–4, and octahedral particles are partially dissolved at $[Au]_1/[Au]_0$ ratios of 2–4 due to the occurrence of shape selective etching by $AuCl_4^-$ + Cl^- anions below ≈160 °C. In this case, shape and size distributions are intermediate between limited cases (a) and (b).

All Au seeds are dissolved into solutions as Au clusters and $AuCl_n^-$ ($n = 4$ and 2) in case (b). In this case, not only the stability of crystal structures for etching but also the number density of Au^0 atoms is an important factor for the final shapes of products. Crystal growth of silver halides, having FCC crystal structures, has been extensively studied due to their application to photographic technologies. According to the modeling of twinning processes during the precipitation of AgBr, the probability of subsequent twinning of an adjoining face must be high for the formation of multiple twin crystals.[34] Such a probability is high when the nuclei is exposed to the twinning environment at high reagent ion concentrations. The probability of twinning is expected to be low, when the number density of Au^0 atoms prepared in solution is small at low $AuCl_4^-$ + Cl^- concentrations. Therefore, single crystal particles, such as octahedral particles, formed by low solution supersaturation, are produced at low $AuCl_4^-$ concentration. On the other hand, single twin and multiple twin particles, formed through instability of high solution supersaturation due to high rate of addition of growth species (Au^0), are preferentially produced at high $AuCl_4^-$ + Cl^- concentrations. This is a major reason for the preferential formation of Au twin crystals in the present systems at high $AuCl_4^-$ + Cl^- concentrations.

We found that decahedral particles were favored at high $AuCl_4^-$ concentrations, whereas icosahedral particles were favored at high Cl^- concentrations. Since the etching rate of Au seeds by $AuCl_4^-$ + Cl^- anions is enhanced in the presence of appropriate amounts of Cl^- anions, more Au^0 atoms are generated by the addition of NaCl. At higher Au^0 concentrations, the probability of the formation of icosahedral particles having more twin planes will be larger than that of decahedral particles. This is the main reason why icosahedral particles are produced predominantly by the addition of NaCl. When Au nanoparticles are prepared in the $AuCl_4^-$/Cl^-/PVP/EG system without the presence of Au seeds, single-twin plate-like particles are dominant particles and multiple-twin decahedral and icosahedral particles are minor or absent.[35] This is attributed to the formation of a lower number density of Au^0 in such a system due to lack of etching of Au seeds by the $AuCl_4^-$ + Cl^- anions.

Conclusion

Seeded growth of anisotropic Au nanoparticles has been studied extensively.[5–8] In general, Au atoms are overgrown on the Au seeds and shapes and sizes of Au seeds do not change during the preparation of anisotropic Au nanoparticles. In the present study, seeded growth of Au nanoparticles was studied by using a MW–polyol method. The present seeded growth system was quite unusual, because the shapes and the sizes of Au seeds changed significantly. It was found that shape selective etching of Au seeds occurred in the Au(seeds)/

$AuCl_4^-$/Cl^-/PVP/EG system. Etching rates of Au seeds were enhanced by adding NaCl. In general, yields of decahedral particles increased at high $AuCl_4^-$ concentrations, whereas those of icosahedral particles became large at appropriate Cl^- concentrations. Spherical and octahedral particles were etched more rapidly than the single-twin and multiple-twin particles, so that they disappeared at high $AuCl_4^- + Cl^-$ concentrations. These shape selective etching of Au seeds by $AuCl_4^- + Cl^-$ anions can be used as a new technique for the shape- and size-controlled synthesis of Au nanocrystals.

It has been believed that Au metal is resistant to oxidative etching. However, we found here that $AuCl_4^-$ from $HAuCl_4$ itself actually etched Au particles in the range of 60–160 °C in the presence of Cl^- and PVP under MW and oil-bath heating. The etching rate of Au seeds in the MW heating was faster than that in the oil-bath heating probably due to the penetration of MW through Au nanoparticles. The shape selectivity of Au nanoparticles in etching process was different from that of Ag: twin crystals were etched and single crystals grew to large particles. In order to clarify why such a drastic difference takes place between Au and Ag, further detailed experimental and theoretical studies on the mechanisms of shape selective crystal growth and oxidative etching of these typical metals are necessary.

Although Au seeds were etched under both MW and oil-bath heating below ≈160 °C, Au nanoparticles obtained by the two methods after heating to 198 °C were significantly different from each other. Highly crystalline polygonal particles were produced at high yields only under MW heating. It was attributed to the interaction of MW with Au nanoparticles leading to local heating of Au particles. In order to confirm the validity of this explanation, further detailed experimental and theoretical studies will also be necessary.

Authors thank Profs. M. Sato and M. Tanaka of Japanese National Institute for Fusion Science for their helpful discussion on effects of MW irradiation for the preparation of metallic nanoparticles on the basis of theoretical simulation and Prof. H. Ago of Kyushu Univ. for the use of his SEM. This work was dedicated to the memory of Koro Tsuji (1992.3.17–2007.5.22). This work was supported by JST-CREST, Joint Project of Chemical Synthesis Core Research Institutions, and Grant-in-Aid for Scientific Research on Priority Areas "unequilibrium electromagnetic heating" and Grant-in-Aid for Scientific Research (B) from the Ministry of Education, Culture, Sports, Science and Technology of Japan (Nos. 19033003 and 19310064).

Supporting Information

Definition of average sizes of each particle, TEM images, size distributions, and absorption spectra of Au nanoparticles and color changes of product solutions are available.

References

1 F. Fievet, J. P. Lagier, B. Blin, B. Beaudoin, M. Fiflarz, *Solid State Ionics* **1989**, *32–33*, 198.

2 a) P.-Y. Silvert, R. Herrera-Urbina, N. Duvauchelle, V. Vijayakrishnan, K. Tekaia-Elhsissen, *J. Mater. Chem.* **1996**, *6*, 573. b) P.-Y. Silvert, R. Herrera-Urbina, K. Tekaia-Elhsissen, *J. Mater. Chem.* **1997**, *7*, 293.

3 M. S. Hegde, D. Larcher, L. Dupont, B. Beaudoin, K. Tekaia-Elhsissen, J. M. Tarascon, *Solid State Ionics* **1996**, *93*, 33.

4 M. Tsuji, M. Hashimoto, Y. Nishizawa, M. Kubokawa, T. Tsuji, *Chem. Eur. J.* **2005**, *11*, 440.

5 M. C. Daniel, D. Astruc, *Chem. Rev.* **2004**, *104*, 293.

6 C. J. Murphy, *Science* **2002**, *298*, 2139.

7 B. Nikoobakht, M. A. El-Sayed, *Chem. Mater.* **2003**, *15*, 1957.

8 a) C. J. Murphy, T. K. Sau, A. M. Gole, C. J. Orendorff, J. Gao, L. Gou, S. E. Hunyadi, T. Li, *J. Phys. Chem. B* **2005**, *109*, 13857. b) C. J. Murphy, A. M. Gole, E. Simona, A. E. Hunyadi, C. J. Orendorff, *Inorg. Chem.* **2006**, *45*, 7544.

9 M. Hu, J. Chen, Z.-Y. Li, L. Au, G. V. Hartland, X. Li, M. Marquez, Y. Xia, *Chem. Soc. Rev.* **2006**, *35*, 1084.

10 M. Tsuji, M. Hashimoto, Y. Nishizawa, T. Tsuji, *Chem. Lett.* **2003**, *32*, 1114.

11 M. Tsuji, M. Hashimoto, Y. Nishizawa, T. Tsuji, *Mater. Lett.* **2004**, *58*, 2326.

12 M. Tsuji, K. Matsumoto, T. Tsuji, H. Kawazumi, *Mater. Lett.* **2005**, *59*, 3856.

13 H. M. Kingston, S. J. Haswell, *Microwave-Enhanced Chemistry, Fundamentals, Sample Preparation, and Applications*, Am. Chem. Soc., Washington DC, **1997**.

14 M. Tsuji, N. Miyamae, K. Matsumoto, S. Hikino, T. Tsuji, *Chem. Lett.* **2005**, *34*, 1518.

15 M. Tsuji, N. Miyamae, S. Lim, K. Kimura, X. Zhang, S. Hikino, M. Nishio, *Cryst. Growth Des.* **2006**, *6*, 1801.

16 a) S. H. Im, Y. T. Lee, B. Wiley, Y. Xia, *Angew. Chem., Int. Ed.* **2005**, *44*, 2154. b) B. Wiley, T. Herricks, Y. Sun, Y. Xia, *Nano Lett.* **2004**, *4*, 1733. c) Y. Sun, Y. Xia, *J. Am. Chem. Soc.* **2004**, *126*, 3892. d) B. Wiley, Y. Sun, Y. Xia, *Langmuir* **2005**, *21*, 8077.

17 J. Rodríguez-Fernández, J. Pérez-Juste, P. Mulvaney, L. M. Liz-Marzán, *J. Phys. Chem. B* **2005**, *109*, 14257.

18 N. R. Jana, L. Gearheart, S. O. Obare, C. J. Murphy, *Langmuir* **2002**, *18*, 922.

19 A. Sánchez-Iglesias, I. Pastoriza-Santos, J. Pérez-Juste, B. Rodríguez-González, F. J. García de Abajo, L. M. Liz-Marzán, *Adv. Mater.* **2006**, *18*, 2529.

20 A. Henglein, *Langmuir* **1999**, *15*, 6738.

21 S. Link, Z. L. Wang, M. A. El-Sayed, *J. Phys. Chem. B* **1999**, *103*, 3529.

22 C. Li, W. Cai, Y. Li, J. Hu, L. Peisheng, *J. Phys. Chem. B* **2006**, *110*, 1546.

23 D. Shechtman, I. Blech, D. Gratias, J. W. Cahn, *Phys. Rev. Lett.* **1984**, *53*, 1951.

24 Z. L. Wang, *J. Phys. Chem. B* **2000**, *104*, 1153.

25 C. Lofton, W. Sigmund, *Adv. Funct. Mater.* **2005**, *15*, 1197.

26 B. Wiley, Y. Sun, B. Mayers, Y. Xia, *Chem. Eur. J.* **2005**, *11*, 454.

27 Y. Gao, P. Jiang, L. Song, L. Liu, X. Yan, Z. Zhou, D. Liu, J. Wang, H. Yuan, Z. Zhang, X. Zhao, X. Dou, W. Zhou, G. Wang, S. Xie, *J. Phys. D.* **2005**, *38*, 1061.

28 M. Tsuji, K. Matsumoto, N. Miyamae, T. Tsuji, T. X. Zhang, *Cryst. Growth Des.* **2007**, *7*, 311.

29 M. Tsuji, N. Miyamae, S. Hikino, to be published.

30 M. Suzuki, M. Tanaka, M. Sato, 6th International Symposium Microwave Effects and Application, **2006**, pp. 93–94.

31 M. Tanaka, M. Sato, *J. Chem. Phys.* **2007**, *126*, 034509.

32 *Application of Microwave Techniques: Study from the Beginning*, Institute of Research and Innovation, Kogyochosakai, Tokyo, 2004, p. 86.

33 a) M. Tsuji, K. Matsumoto, P. Jiang, R. Matsuo, X. L. Tang, K. S. N. Kamarudin, *Colloids Surf., A*, in press. b) M. Tsuji, M. Nishio, P. Jiang, N. Miyamae, S. Lim, K. Matsumoto, D. Ueyama, X. L. Tang, *Colloids Surf., A*, submitted.

34 a) R. Jagannathan, *J. Imaging Sci.* **1991**, *35*, 104. b) R. Jagannathan, V. V. Gokhale, *J. Imaging Sci.* **1991**, *35*, 113.

35 M. Tsuji, N. Miyamae, M. Hashimoto, M. Nishio, S. Hikino, I. Tanaka, *Colloids Surf., A* **2007**, *302*, 587.